Fuel 279 (2020) 118491

Contents lists available at ScienceDirect

Fuel

journal homepage: www.elsevier.com/locate/fuel

Full Length Article

Soot inception: A DFT study of σ and π dimerization of resonantly stabilized aromatic radicals

Francesco Silvio Gentile[a,b], Francesca Picca[a,*], Gianluigi De Falco[a], Mario Commodo[c,*], Patrizia Minutolo[c], Mauro Causà[a], Andrea D'Anna[a]

[a] Dipartimento di Ingegneria Chimica, dei Materiali e della Produzione Industriale – Università degli Studi di Napoli Federico II, P.le Tecchio 80, 80125 Napoli, Italy
[b] Dipartimento di Chimica – Università degli Studi di Torino, Via Giuria 5, 10125 Torino, Italy
[c] Istituto di Ricerche sulla Combustione, CNR, P.le Tecchio 80, 80125 Napoli, Italy

ARTICLE INFO

Keywords:
Soot
Polycyclic aromatic hydrocarbons
Radicals
Density functional theory

ABSTRACT

Recent advances in the soot studies have shown experimental evidences of π-radicals and cross-linked structures among the molecular constituents of just-nucleated soot particles. π-radicals could have an important role in particle nucleation by increasing the binding energy between polycyclic aromatic hydrocarbons with respect to pure van der Waals interactions. In this work we use density functional theory by Grimme D3 dispersion correction (DFT-D3) with hybrid functional and localized Gaussian basis set (B3LYP/6-31G**) to analyze and classify the clustering behaviors of two aromatic radicals visualized experimentally by atomic force microscopy (Commodo et al. *Combust. Flame* 205: 154–164, 2019). These aromatic radicals have different topological structures and delocalization of the unpaired electron. The binding energy and energy bandgap characteristics of the clusters are calculated. The theoretical results show a different clustering behavior for the two aromatic radicals. The one with a partial localization of the unpaired electron tends to form a σ-dimer; conversely, the radical with a greater delocalization of the unpaired electron leads to π-stacking formation with a slight overbinding of few kcal mol^{-1} with respect to pure van der Waals interactions and a marked lowering of the energy bandgap. The formation of π-stacking induced by delocalized π-radicals could in part explain some spectroscopic evidences observed during soot nucleation.

1. Introduction

The formation of soot and condensed-phase carbonaceous materials in flames is an area of ongoing research strongly motivated by the adverse health effects of the emitted particles and the complex implications they have to the climate change [1–4]. Moreover, in recent years, it has been shown that soot, and carbon nanoparticles in general, thanks to their optical and electronic properties, are interesting low-cost materials to be used in a variety of applications, including energies harvesting as solar cell material [5,6] and energy storage [7]. Carbon nanoparticles have proven also to be a promising light-emitting nanomaterial showing remarkable photoluminescence properties [8,9] and quantum confinement behaviors [10].

An accurate tuning of the properties of flame-formed nanoparticles requires a deep knowledge of their formation mechanisms, particularly of the early stages of the nucleation process. Moreover, understanding of the particle inception process is also crucial to develop low-emission, cleaner combustion technologies.

It is generally agreed that polycyclic aromatic hydrocarbons (PAHs) play an important role in soot nucleation and growth; they are ubiquitous by-products of fuel-rich flames that survive from fragmentation at high temperature due to the high stability of the six-membered benzenoid rings [11]. The most stable individual molecules are organized in pericondensed systems; examples are naphthalene, phenantherene, pyrene and coronene, and even larger pericondensed aromatics. In addition to the purely benzenoid PAHs, five-member rings are also present and they seem to have a controlling role in the formation and growth of aromatic. Acenaphthylene-type rings, i.e., acenaphthylene and cyclopenta(cd)pyrene, are formed in flames due to their high stability as predicted by Fahr and Stein [11]. This type of pentagonal ring can be rapidly formed by hydrogen abstraction followed by acetylene (C_2H_2) addition on a zigzag edge of an aromatic structure as computationally observed by Frenklach and coworkers in a series of earlier investigations [12–14]. In a combined experimental and computational study, Johansson et al. [15], suggested, for the soot-precursor structures, a relevant contribution of five-membered rings, as

* Corresponding authors.
E-mail addresses: francesca.picca@unina.it (F. Picca), commodo@irc.cnr.it (M. Commodo).

https://doi.org/10.1016/j.fuel.2020.118491
Received 22 September 2019; Received in revised form 20 April 2020; Accepted 19 June 2020

opposed to only six-membered rings. However, only the recent use of high-resolution atomic force microscopy (HR-AFM), succeed in providing a definitive assessment on the contribution and type of pentagonal rings in the incipient soot molecules [16,17].

Other than acenaphthylene-type rings, a large variety of cross linked bi-phenyl-, fluorene- and fluoranthene-like PAHs have also been detected at the soot inception in laminar premixed flame [16,17]. Notably, a remarkable number of PAHs containing pentagonal rings or even six-membered rings with methylene groups (–CH_2-) were also detected [16,17].

H atom abstraction to –CH_2- of the partially protonated rim-based pentagonal rings and/or H atom addition to acenaphthylene-type *cyclo*-penta rings form delocalized π radicals. Indeed, if an H atom is removed from the aromatic molecule composed by purely benzenoid rings, the unpaired electron occupies an orbital lying in the plane of the local molecular framework, thus forming a σ radical. Conversely, if a H atom is removed from an sp^3 hybridized carbon at the periphery of an aromatic molecule, such as a –CH_2- group in a five-membered or six-membered ring of a PAH, or a H atom is added to an unsaturated ring, the unpaired electron occupies an orbital perpendicular to the local molecular framework, thus forming a π radical which delocalizes over the entire molecule [18].

Unpaired electrons in orbitals lying in the plane (σ radicals) are unable to be delocalized on the aromatic system: it is the case of a phenyl radical. In the molecular growth mechanism by acetylene (HACA mechanism), these σ radicals undergo sequential reactions of acetylene addition leading to the formation of larger aromatics [12]. The self-combination of these types of radicals forms bi-phenyl like, cross-linked compounds [19].

An unpaired electron located in an orbital perpendicular to the plane, π radical, is able to be delocalized through the entire molecule and stabilizes by resonance. In addition to be critical for the formation of the first aromatic ring [20], the resonantly stabilized π radicals have long been considered important species in promoting soot nucleation and growth [21,22], and recently they have been experimentally observed by Johansson et al. [23] using photoionization mass spectrometry. Furthermore, resonantly stabilized π radicals were clearly observed by HR-AFM [16,17], and more recently detected by electron paramagnetic resonance (EPR) spectroscopy measurements [24].

On the bases of these new experimental evidences, it has been speculated that resonantly stabilized π radicals, mainly due to partially protonated rim-based pentagonal rings, might be involved in the nucleation/clustering of aromatics, promoting bridging reactions [25,26], to form three-dimensional carbon structures. The role of resonantly stabilized radicals in aromatic growth and soot inception was already hypothesized by D'Anna et al. [27].

Aromatic radicals are known to play a fundamental role in numerous branches of organic chemistry; one of the most investigated aromatic π radical compound, the phenalenyl radical, has been found to form π-stacking intermolecular attraction, sometime referred to as "pancake bond" or "multi-electron/multi-center (me/mc)" consisting on an unusual delocalized covalent-like bond [28,29].

In this work we analyze the dimerization process of PAH molecules and radicals recently identified as building-blocks of just nucleated soot particles. We performed density functional theory DFT-D3 calculations, with hybrid functional and localized Gaussian basis set (B3LYP/6-31G**), to study the interactions of two π-PAH radicals found in the ensemble of soot molecular constituents visualized by HR-AFM [17], named in the following R1 and R2 (IS1 and IS13 in Ref. [17]). We calculate the DFT-D3 structures of single radicals and of their dimers in order to assess the role of radical aggregation on the inception of soot particles. The Mulliken population analysis (MPAN) of the spin density [30], has been used to understand the effect of the radical delocalization value on different dimerization pathways.

Finally, an analysis of the two different dimerization processes, in term of binding energy and spectroscopic behaviors (band gap), has been also performed.

2. Computational method

Calculations have been performed by using the DFT-D3 approach with a linear combination of atomic orbital (LCAO). All systems are treated with the use of unrestricted spin polarized method. The Hamiltonian adopted is the B3LYP global hybrid functional [31] as implemented in the Crystal17 program [32]. All-electron 6-31G** double zeta split valence plus polarization basis set of Gaussian-type functions, centered on the nuclei, has been adopted for C, the number of atomic orbitals span from 457 to 505 in isolated radical cases and the twice (from 914 to 1010) in the dimer cases.

The asymmetric geometry of the studied compounds produces a C_1 point symmetry. The truncation of Coulomb and exchange series is controlled by five thresholds Ti (see Crystal manual [33], for more details), which have been set to 8 (T1-T3), 12 (T4) and 50 (T5), for a correct evaluation of the exchange interactions. The convergence threshold on energy for the self-consistent-field (SCF) procedure has been set to 10^{-8} Hartree for structural optimizations. The convergence criteria of the route mean square (RMS) of the analytical gradient and the displacement were tightened, from the default values of 0.0003 a.u. and 0.0012 a.u. to 0.0001 a.u. and 0.0004 a.u., respectively, to provide accurate geometry optimizations of the final structures. The DFT exchange–correlation contribution to the Fock matrix has been evaluated by numerical integration over the molecular volume. Radial and angular points for the integration grid are generated through Gauss-Legendre radial quadrature and Lebedev two-dimensional angular point distributions. The default pruned grid XLGRID with 75,974 points (75 radial and 974 angular points) has been increased to a very dense XXLGRID with 991,454 points (99 radial and 1454 angular points), whose accuracy can be measured by comparing the integrated charge density considered Ni = 393.9996 electrons, with the total number of 394 electrons in the molecule. The dispersion interactions are evaluated using "Grimme" D3 scheme method [34].

The classical dispersion energy is sum of the DFT energy using a weight function that avoids double counting of the short-range interactions. The electron 3D spatial extension of the electron and spin densities have been calculated integrating the wave function obtained from SCF calculations in a dense spatial point.

All dimerization energies have been reported without taking into account the counterpoise correction (CC), usually employed for the evaluation of the basis set superposition error (BSSE). The BSSE energy corrections span in a range from +7 to +8 kcal mol^{-1} (as reported in Table 2 it is evaluated for the case of not covalently bonded D_{R2} dimer in different geometries) but they do not change the trends of the dimerization energies. The approach used is not the most accurate if it is applied to a small or medium size molecules, but it allows performing agile and reliable calculations on moderately large models, as are those investigated in this work, and it is easily extendable to molecules with one thousand atoms and more.

In order to estimate the quality of our results about the energy dimerization, a benchmark involving small aromatic dimers is reported in the Supplemental Material. The domain-based local pair natural orbital coupled cluster method with single, double and perturbative estimation of triples excitations -DLPNO-CCSD(T)- has been chosen as a reference method, employing ORCA 4.2.1 software [35]. In DLPNO-CCSD(T) calculation a triple ζ basis set with two set of polarization functions def2-TZVPP has been adopted [36].

2.1. Mulliken population analysis of the spin density

For very large and complex molecular systems, a clear discrimination between the two types of radicals, i.e., σ and π radical, may not be a trivial task. In these cases, a helpful way to differentiate between the two kinds of radicals is to use the Mulliken population analysis (MPAN)

of the spin density, i.e., the electron density of the free electrons [30]. MPAN investigates the distribution of electronic spin within a system. To this end, the spin up (α) and spin down (β) electronic populations are analysed separately and their sums ($\alpha + \beta$) and differences (α-β) are evaluated to yield the charges and net spins of the system, respectively. Such analysis is very helpful in providing where the unpaired electron is located for an assigned molecular structure. Although the MPAN determination of the spin density suffer of some degree of inaccuracy that arises from the equal division of the off-diagonal terms in the matrices (P•S), it offers acceptable results for a comparison perspective, especially in these covalent systems.

In σ-aromatic radical, the spin population is concentrated almost totally, more than 92%, on the carbon atom close to the dangling bond (atom with an unsatisfied valence). For the π-aromatic radical, the spin population is distributed over the carbon rings (in alternate topology) and the maximum localization over single carbon atoms does not exceed 35–40%.

3. Results and discussion

Before analyzing two characteristic soot component radicals identified by HR-AFM [16,17], we have performed preliminary calculations on the phenalenyl radical self-combination, a mechanism that has been largely studied in the literature. These preliminary calculations are useful to test the capability of the used approach to reproduce previous theoretical and experimental studies.

Phenalenyl, sketched in Fig. 1, is a π radical as also confirmed by spin MPAN: 31% of spin density on the equivalent peripheral carbon atoms; 15% on the semi-peripheral Carbon atoms; 7% at the central site.

The peculiarity of this radical lies in its self-combination capability through the formation of two types of dimers: σ- and π-dimer. The σ-dimer shows a single C–C bond between peripheral carbon atoms of the two radicals; the two molecules do not overlap as shown in Fig. 1 (right side). The dimerization energy is 12.9 kcal mol^{-1}, calculated with respect to the two separated phenalenyl radicals in reasonable agreement with literature data, 10 kcal mol^{-1} [37]. The π-dimer has two different configurations: in the first one the two radicals exactly overlap whereas in the second configuration, shown in Fig. 1 left side, the two radicals present an inversion center (head–tail configuration) and a shift of the polyaromatic rings giving a staggered “graphite” like structure. Our calculations show the perfectly overlapped stacking dimer to be 13.6 kcal mol^{-1} more stable than the monomers in unrestricted open shell singlet electronic configuration and 9.7 kcal mol^{-1} in the triplet state. The π-dimer in head–tail graphite-like configuration is more stable than the σ-dimer; its interaction energy is of 22.3 kcal mol^{-1}, a value higher than that calculated at coupled cluster level [28].

Based on this test-case, we have extended our computational effort to larger molecular models based on the experimental observations of the molecular constituent of incipient soot [16,17]. Therefore, the two radical PAHs, named R1 and R2, and sketched in Fig. 2, are examined in this study.

The radicals have been preliminary studied as individual structures. In principle, these molecules are π radicals since the electron of the dangling bond is not univocally localized in one specific atom site on the molecular plane, thus the unpaired electron is hosted by molecular orbitals belonging to the π system. Fig. 2 (top panel) reports the calculated 0.001 electrons/bohr3 *iso*-level of the electronic density, projected in the singly occupied molecular orbital (SOMO) range energy, in R1 and R2, respectively. It provides a topological representation of the magnetic behavior of the molecules. Note that, this classical representation does not correspond to the physical position of the unpaired electron. Indeed, this latter is provided by MPAN that gives, in a first approach, the formal charges and spin densities, whose results are reported in Table 1 and also shown in Fig. 2 (lower panel) as colored dots highlighting the carbons with higher (red-label) and lower (blue-label) spin orbital contribution.

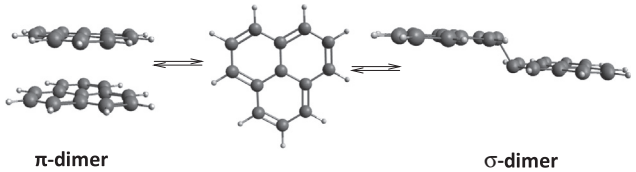

Fig. 1. Scheme of phenalenyl radical dimerization.

R1 radical has a hybrid behavior, due to its peculiar topology, showing a low delocalization of the unpaired electron. The carbon atom belonging to the non-aromatic ring (C25) shows a spin population $\mu = 0.67$ |e| (see Table 1), thus indicating a noticeable localization of the unpaired electron. It is also possible to find a second localization site, namely C11 (in alternate position with respect to C25), which has a spin population $\mu = 0.41$ |e| (Fig. 2 and Table 1). We could define this type of radical as a partially localized π-radical, whose role in the aggregation/clustering, through an enhanced binding in PAHs clusters, was formerly postulated by Wang [38], and in a recent DFT study thoroughly discussed by Martin et al. [25].

By contrast, the R2 radical can be considered as a pure π radical; indeed, the maximum localization does not exceed a spin population value of 0.42 |e| over a single site (C11) while the other two with largest spin population are equally spanned among other two sites (C1 and C3, see Fig. 2 and Table 1). The delocalization of the unpaired electron, more specifically the spin population, was observed to be higher on peripheral carbon sites than the central ones.

The different delocalization of unpaired electrons in R1 and R2 radicals produces a substantial difference in dimer formation. Dimers of R1 radicals, D_{R1}, always form a single bond between the carbon atoms, hosting the localized unpaired electron. The bond length is 1.603 Å, while the two poly-aromatic structures are slightly bent, as shown in the dimer equilibrium geometry reported in Fig. 3, in which the calculated 0.001 electrons/$bohr^3$ isolevel of the electronic density in D_{R1} and R2 dimers, D_{R2}, in both spin multiplicity, are reported.

To study the energetic contribution of the open shell configuration in aromatic dimerization we compared the calculated interaction energy of the D_{R1} and the corresponding closed shell M1 molecule sketched in Fig. 4. Indeed, D_{R1} can be formed by H atom abstraction from the partially protonated rim-based pentagonal ring of molecule M1 (backward reaction in Fig. 4 upper panel).

The calculated interaction energy for M1 dimer, D_{M1}, is about 30 kcal mol^{-1}. We can assume that this value is representative of purely van der Waals interactions. The interaction energy in D_{R1} is 71.7 kcal mol^{-1}. Therefore, assuming that the van der Waals interactions accounts for the same energy value for both D_{R1} and D_{M1} dimer, we can estimate that the σ bond contributes with about 40 kcal mol^{-1}, corresponding to a weak single C—C bonds.

For D_{R2}, different geometries, and spin multiplicities need to be considered. Particularly, three geometries have been explored as reported in Fig. 5:

- radicals perfectly overlapped;
- radicals shifted in a graphite staggered like structure;
- radicals in head–tail configuration.

In Table 2 the interaction energies for D_{R2} in the three geometries and in singlet and triplet multiplicity states are reported.

It is worth noticing that D_{R2} triplet multiplicity does not present the overlapped equilibrium geometry due to electronic repulsion. In D_{R2}, the π electronic densities tend to overlap, as shown in Fig. 3; with a distance between the two stacked molecules that ranges from 3.40 to 3.60 Å, considering both the singlet and triplet state, with an average distance of 3.45 Å for the stack in singlet state and an average distance of 3.58 Å for the stack in triplet state. Calculated distances are reported

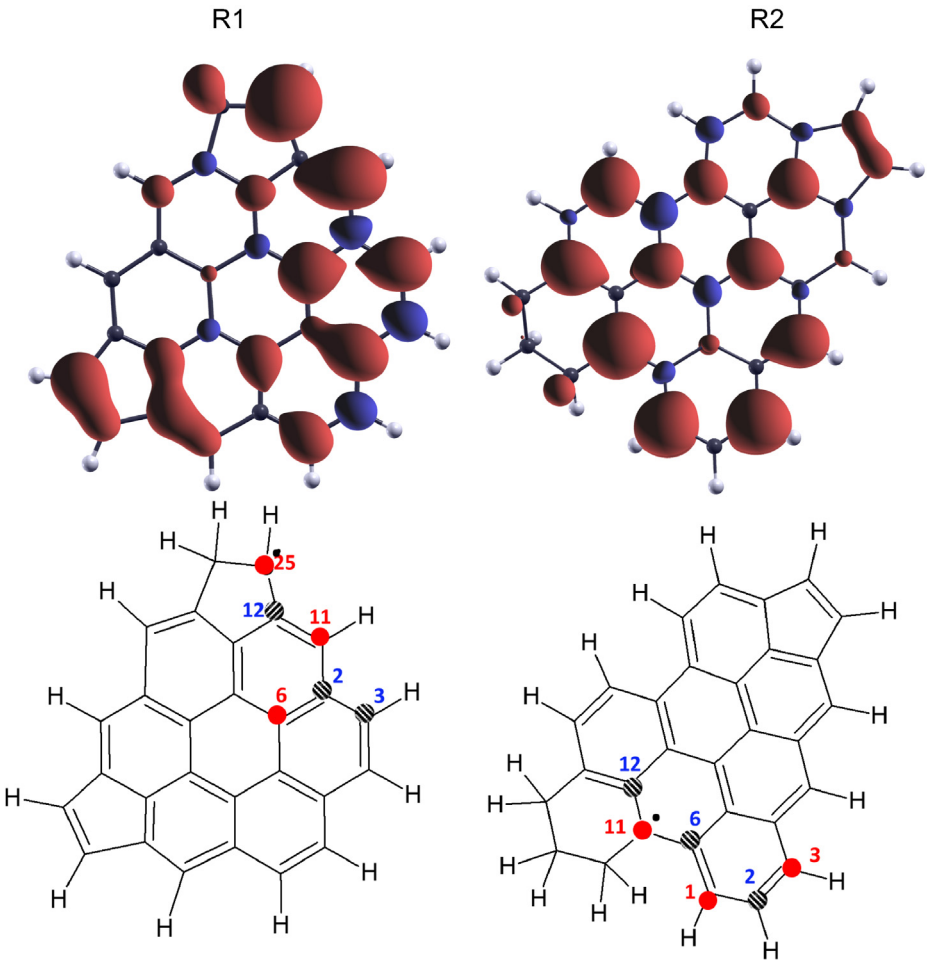

Fig. 2. Investigated R1 and R2 radicals; Top panel: the spin isodensity surface projected only over the SOMO orbital. The surface ranges are evaluated at 0.001 $|e|/(a_0)^3$ isodensity. Red surface are positive values, while blue are negatives; Lower panel: the molecular sketch, in which the small black dot is one of possible resonance representations of the unsaturated site (carbon dangling bond). The circles (with atomic label) indicate the carbon atoms with the higher (positive) values of the MPAN of spin distribution. The striped circles indicate the carbon atoms with the lower (negative) values of the MPAN (values reported in Table 1). (For interpretation of the references to colour in this figure legend, the reader is referred to the web version of this article.)

Table 1
MPAN: Atomic net charge, ρ, and spin population, μ, values for R1 and R2 radicals. All charges are expressed in electron fractions |e|.

C Atom (R1)	ρ(R1)	μ(R1)	C Atom (R2)	ρ(R2)	μ(R2)
2	0.13	−0.13	1	−0.17	0.33
3	−0.14	−0.08	2	−0.08	−0.15
6	0.06	0.18	3	−0.16	0.31
11	−0.23	0.41	6	0.09	−0.17
12	0.21	−0.21	11	0.00	0.42
25	−0.19	0.67	12	0.04	−0.14

in detail in Table 2.

As for D_{R1}, we compare the interaction energy of the most stable D_{R2}, i.e., head–tail configuration in triplet state, to the interaction energy of the dimer of closed shell M2 molecule, D_{M2}, (Fig. 4). A value of −35.8 kcal mol^{-1} was calculated for the D_{M2}, and again we assumed that the interaction is purely due to van der Waals forces. Therefore, the interaction energy of the most stable D_{R2} is just few kcal mol^{-1} (2–4 kcal mol^{-1}) larger than the interaction energy of the D_{M2} indicating a weak multi-center π-π orbital interaction.

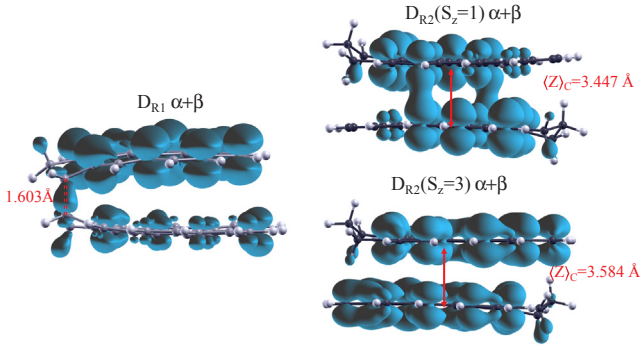

Fig. 3. Calculated 0.001 electrons/bohr^3 isolevel of the electronic density in D_{R1} and D_{R2} dimers. $< Z >_C$ is the average distance between top and bottom carbon atoms z-coordinates. D_{R1} (left): the dashed line shows the distance of the C–C covalent bond; the two bonded C-atoms are sp^3 hybridized D_{R2} (right): the D_{R2} head–tail structures representing the more stable energetic configurational isomer in singlet (top) and triplet state (bottom).

Table 2
Interaction energies and distances between molecules for three geometries and two multiplicity state of D_{R2}. All energies are reported without taking into account the BSSE corrections. The BSSE evaluation increase the interaction energies of in a range from +7 to +8 kcal mol^{-1}.

D_{R2} configurations	Sz = 1 interaction energy [kcal mol^{-1}]	Sz = 3 interaction energy [kcal mol^{-1}]	Sz = 1 Distance [Å]	Sz = 3 Distance [Å]
Overlapped	−28.6	–	3.379	
Staggered	−31.1	−33.5	3.450	3.674
Head-tail	−33.7	−36.8	3.512	3.495

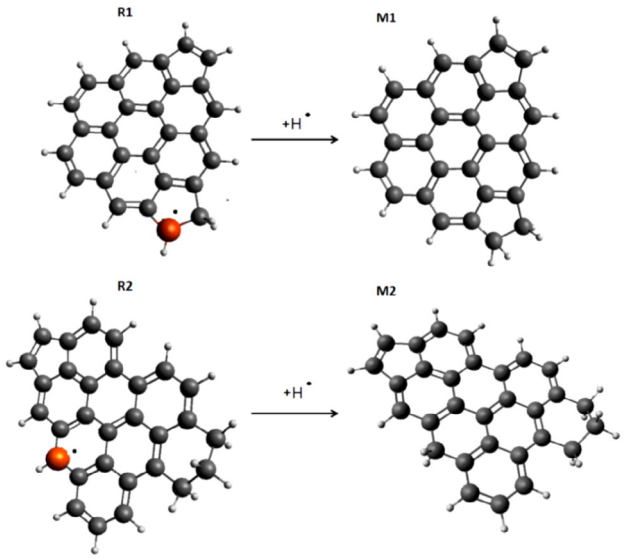

Fig. 4. Equilibrium molecular structures of M1 and M2 closed shell molecules, derived from the R1 and R2 radicals. Radicals are formed by H atom abstraction from the partially protonated rim-based pentagonal ring of the molecules. The largest red spheres indicate the carbon atom of the original radical where the hydrogen atom has been added. (For interpretation of the references to colour in this figure legend, the reader is referred to the web version of this article.)

The above analysis about the interaction energy of the two radical dimers and the equilibrium geometry allows concluding that polycyclic aromatic radicals may form π stacking if the unpaired electron is sufficiently delocalized, which gives a slight overbinding in the cluster interaction with respect to pure van der Waals interactions. When the topology of the molecule causes some spin localization, like in the R1 case, a C—C covalent bond is formed among the localization sites.

3.1. Electronic bandgap calculations

The electronic band gap is an important quantity that characterizes semiconductors and it is widely used for nanostructured materials investigations. However, measured band gap strongly depends on the experimental method. For instance, optical, electrochemical, electrical band gap may show slight differences since they monitor different processes [39]. Theoretically, the band gap is the difference between the highest occupied molecular orbital (HOMO) and the lowest unoccupied molecular orbital (LUMO). Although, B3LYP has been shown to over predict the measured optical band gap [40], the HOMO-LUMO gap (Eg) resulting from our model gives correct trends with respect to gaps calculated at higher theory levels and the method is applicable to large polycyclic aromatic models. Recently, it has been reported in the literature a correlation between PAHs characteristics and their optical band gap, OBG [41,10]. PAH size, structural symmetry, cross-linking, curvature due to pentagonal-ring, radical presence, all these characteristics cause a variation on the OBG of PAHs [40]. In light of this, one of the main objectives of the present study is to deepen the analysis of the effect of the supramolecular assemblies of the polycyclic aromatic molecules and radicals on the HOMO-LUMO gap. To this aim, the energy gap between occupied and unoccupied electronic states has been evaluated for both open and closed shell investigated dimers.

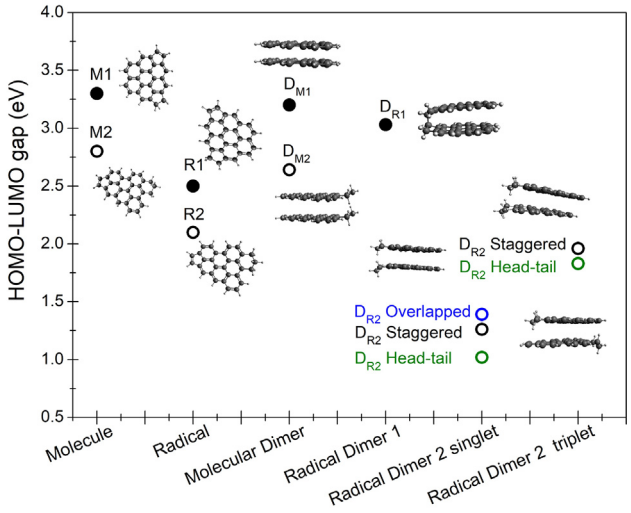

Fig. 6. Calculated HOMO-LUMO gaps.

This computational investigation is aimed to shed light on some experimental observations indicating a typical value of the energy gap for just-nucleated soot particles which is of the order of 1.5–2 eV (34.6–46 kcal mol^{-1}) [42], thus significantly lower than the typical energy gap of the constituent aromatic molecules.

The results of DFT-D3 calculation in terms of energy gap are reported in Fig. 6. M1 molecule has a HOMO-LUMO gap of approximatively 3.3 eV (76.1 kcal mol^{-1}) that decreases when considering the SOMO-LUMO gap of the corresponding R1 radical, i.e., 2.5 eV (57.65 kcal mol^{-1}). A similar trend is also obtained for the corresponding dimers, D_{M1}: the molecular dimer presents an energy gap of 3.2 eV (73.79 kcal mol^{-1}) while the radical dimer, i.e., the σ-bonded D_{R1}, has a gap of 3.03 eV (69.87 kcal mol^{-1}).

M2 molecule has a gap of 2.8 eV (64.57 kcal mol^{-1}), while the gap of the corresponding R2 radical is 2.1 eV (48.43 kcal mol^{-1}). The stack constituted by two M2 molecules, i.e., D_{M2}, has a 2.6 eV (59.96 kcal mol^{-1}) gap, slightly lower than the M2 molecule alone. In the dimer configuration of D_{R2} the orientation of the stacks might further affect the HOMO-LUMO gaps. Indeed, the triplet electronic structures have higher gaps than the singlet ones. Specifically, the D_{R2} in overlapped geometry has an energy gap of 1.39 eV (32.05 kcal mol^{-1}); the D_{R2} in staggered geometry has an energy gap of 1.26 eV (29.06 kcal mol^{-1}) for singlet multiplicity state and 1.96 eV (45.20 kcal mol^{-1}) for the triplet one; D_{R2} for head–tail configuration has an energy gap of 1.02 eV (23.52 kcal mol^{-1}) for singlet and 1.83 eV (42.20 kcal mol^{-1}) for triplet. This behavior is explained by the parallel spin electron repulsion due to the exchange interaction in triplet configuration that decreases the coulombic repulsion causing a stabilization of the HOMO and a consequent increase of the bandgap. It is evident from our calculations that the presence of delocalized π unpaired electrons sensibly decreases the HOMO-LUMO gap. Therefore, the stacking of polycyclic aromatic radicals decreases the HOMO-LUMO gap by a quantity that is dependent on the geometry of aggregation and spin multiplicity.

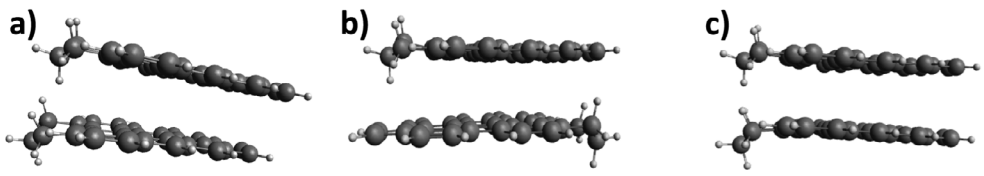

Fig. 5. a) D_{R2} Staggered geometry; b) D_{R2} Head-tail geometry; c) D_{R2} Overlapped geometry.

4. Conclusion

DFT-D3 calculations of the self-association of two π-radicals and the corresponding molecules have been performed. The radicals differ each other for a different level of delocalization of the unpaired electron over the aromatic framework. This difference is crucial in determining the dimerization process, the binding energy, and energy band gap characteristic of the clustering of two different molecular radicals.

Based on MPAN calculations, our results show that π radicals with a partial localization tend to form a σ-dimer. The σ-dimer is characterized by longer length and weaker energy bond than a standard σ-bond. On the other hand, our calculations showed that π radicals with a greater delocalization of the unpaired electron lead to π-stacking formation. The interaction energy of this dimer resulted prevalently due to Van der Waals contributions, however, an additional interaction energy, attributed to multi-electron/multi-center bond, has been estimated.

Another relevant result of the present computational work is the evaluation of the effects of delocalization of the unpaired electron and type of dimerization process on the HOMO-LUMO gap. We can assert that the formation of a radical leads to a lowering of the optical bandgap. The HOMO-LUMO gap further decreases as they form dimers. The obtained gap values are different based on the molecular geometry of the stacked structures and on their spin-multiplicity. Nevertheless, the formation of π-stacking induced by delocalized π-radicals could in part explain some spectroscopic evidences observed during soot nucleation [43,44].

According to the experiments, soot particles are composed by an ensemble of PAH whose typical size are of the order of ovalene, 1 nm. However, the optical band gap measured for nascent soot particles is commonly much lower than the corresponding cluster of pure ovalene and other characteristic aromatic molecules [10,41,45]. To this regard, the presence of radicals and their dimers into a soot particle may explain such discrepancies. Further work is needed to better understand the role of interactions involving radical compounds also considering a broader set of molecule and radical precursors of soot.

CRediT authorship contribution statement

Francesco Silvio Gentile: Software, Validation, Formal analysis, Writing - original draft, Writing - review & editing. **Francesca Picca:** Investigation, Writing - original draft, Writing - review & editing. **Gianluigi De Falco:** Investigation, Writing - original draft, Writing - review & editing. **Mario Commodo:** Conceptualization, Investigation, Writing - original draft, Writing - review & editing. **Patrizia Minutolo:** Investigation, Writing - original draft, Writing - review & editing. **Mauro Causà:** Software, Validation, Formal analysis, Writing - original draft, Writing - review & editing. **Andrea D'Anna:** Supervision, Conceptualization, Writing - original draft, Writing - review & editing.

Declaration of Competing Interest

The authors declare that they have no known competing financial interests or personal relationships that could have appeared to influence the work reported in this paper.

Acknowledgment

The authors acknowledge the financial support from the PRIN project 2017PJ5XXX: "Modeling and Analysis of carbon nanoparticles for innovative applications Generated dIrectly and Collected DUring combuSTion (MAGIC DUST)".

Appendix A. Supplementary data

Supplementary data to this article can be found online at https://doi.org/10.1016/j.fuel.2020.118491.

References

[1] Lighty JS, Veranth JM, Sarofim AF. Combustion aerosols: factors governing their size and composition and implications to human health. J Air Waste Manage Assoc 2000;50:1565–618.
[2] Pedata P, Stoeger T, Zimmermann R, Peters A, Oberdörster G, D'Anna A. Are we forgetting the smallest, sub 10 nm combustion generated particles? Part Fibre Toxicol 2015;12:34.
[3] Bond TC, Doherty SJ, Fahey DW, Forster PM, Berntsen T, DeAngelo BJ, et al. Bounding the role of black carbon in the climate system: a scientific assessment. J Geophys Res [Atmos]. 2013;118:5380–552.
[4] Hansen J, Nazarenko L. Soot climate forcing via snow and ice albedos. Proc Natl Acad Sci 2004;101:423–8.
[5] Wei Z, Yan K, Chen H, Yi Y, Zhang T, Long X, et al. Cost-efficient clamping solar cells using candle soot for hole extraction from ambipolar perovskites. Energy Environ Sci 2014;7:3326–33.
[6] Bruno A, Commodo M, Haque SA, Minutolo P. Spectroscopic investigation of flame synthesized carbon nanoparticle/P3HT blends. Carbon 2015;94:955–61.
[7] Kakunuri M, Sharma CS. Candle soot derived fractal-like carbon nanoparticles network as high-rate lithium ion battery anode material. Electrochim Acta 2015;180:353–9.
[8] Ray SC, Saha A, Jana NR, Sarkar R. Fluorescent carbon nanoparticles: synthesis, characterization, and bioimaging application. J Phys Chem C 2009;113:18546–51.
[9] Rahy A, Zhou C, Zheng J, Park SY, Kim MJ, Jang I, et al. Photoluminescent carbon nanoparticles produced by confined combustion of aromatic compounds. Carbon 2012;50:1298–302.
[10] Liu C, Singh AV, Saggese C, Tang Q, Chen D, Wan K, et al. Flame-formed carbon nanoparticles exhibit quantum dot behaviors. Proc Natl Acad Sci 2019;116(26):12692–7.
[11] Stein SE, Fahr A. High-temperature stabilities of hydrocarbons. J Phys Chem 1985;89(17):3714–25. https://doi.org/10.1021/j100263a027.
[12] Frenklach M, Clary DW, Gardiner Jr. WC, Stein SE. Detailed kinetic modeling of soot formation in shock-tube pyrolysis of acetylene. Symp Int Combust Proc 1985;20:887–901.
[13] Frenklach M, Schuetz CA, Ping J. Migration mechanism of aromatic-edge growth. Proc Comb Inst 2005;37:1389–96.
[14] Whitesides R, Frenklach M. Detailed kinetic Monte Carlo simulations of graphene-edge growth. J Phys Chem A 2010;114(2):689–703.
[15] Johansson KO, Dillstrom T, Elvati P, Campbell MF, Schrader PE, Popolan-Vaida DM, et al. Radical–radical reactions, pyrene nucleation, and incipient soot formation in combustion. Proc Combust Inst 2017;36:799–806.
[16] Schulz F, Commodo M, Kaiser K, De Falco G, Minutolo P, Meyer G, et al. Insights into incipient soot formation by atomic force microscopy. Proc Combust Inst 2019;37:885–92.
[17] Commodo M, Kaiser K, Schulz F, De Falco G, Minutolo P, D'Anna A, et al. On the early stages of soot formation: molecular structure elucidation by high-resolution atomic force microscopy. Combust Flame 2019;205:154–64.
[18] Howard JB. Carbon addition and oxidation reactions in heterogeneous combustion and soot formation. Symp (Int) Combust 1991;23:1107–27.
[19] D'Anna A, Violi A, D'Alessio A, Sarofim AF. A reaction pathway for nanoparticle formation in rich premixed flames. Combust Flame 2001;127:1995–2003.
[20] Miller JA, Melius CF. Kinetic and thermodynamic issues in the formation of aromatic compounds in flames of aliphatic fuels. Combust Flame 1992;91:21–39.
[21] Homann KH, Wagner H Gg. Some new aspects of the mechanism of carbon formation in premixed flames. Symp (Int) Combust 1967;11:371–9.
[22] Keller A, Kovacs R, Homann K-H. Large molecules, ions, radicals and small soot particles in fuel-rich hydrocarbon flames. Part IV. Large polycyclic aromatic hydrocarbons and their radicals in a fuel-rich benzene–oxygen flame. PCCP 2000;2:1667–75.
[23] Johansson KO, Head-Gordon MP, Schrader PE, Wilson KR, Michelsen HA. Resonance-stabilized hydrocarbon-radical chain reactions may explain soot inception and growth. Science 2018;361:997–1000.
[24] Vitiello G, De Falco G, Picca F, Commodo M, D'Errico G, et al. On the relevance of radicals in carbon clustering and soot inception: a joint EPR and Raman spectroscopy study. Combust Flame 2019;205:286–94.
[25] Martin JW, Hou D, Menon A, Pascazio L, Akroyd J, You X, et al. Reactivity of Polycyclic Aromatic Hydrocarbon Soot Precursors: Implications of Localized p-Radicals on Rim-Based Pentagonal Rings. J Phys Chem C 2019;123(43):26673–82.
[26] Frenklach M, Mebel AM. On the mechanism of soot formation. PCCP 2020;22:5314–31.
[27] D'Anna A, Violi A, D'Alessio A. Modeling the rich combustion of aliphatic hydrocarbons. Combust Flame 2000;121:418–29.
[28] Kertesz M. Pancake bonding: an unusual Pi-stacking interaction. Chem Eur J 2019;25:400–16.
[29] Gao FW, Zhong RL, Sun SL, Xu HL, Su ZM. Two-electron/24-center (2e/24c) bonding in novel diradical π-dimers. PCCP 2016;18:2904.
[30] Mulliken RS. Electronic Population Analysis on LCAO–MO Molecular Wave Functions. I. J. Chem. Phys. 1955;23:1833–40.
[31] Becke AD. A new mixing of Hartree-Fock and local density-functional theories. J Chem Phys 1993;98:1372–7.
[32] Dovesi R, Erba A, Orlando R, Zicovich-Wilson C, Civalleri B, Maschio L et al. Quantum-mechanical condensed matter simulations with CRYSTAL. Wiley Interdisciplinary Reviews: Computational Molecular Science; 2018.

[33] Dovesi R, Saunders VR, Roetti C, Orlando R, Zicovich-Wilson CM, Pascale F, et al. CRYSTAL14 User's Manual; 2014.
[34] Grimme S, Hansen A, Brandenburg JG, Bannwarth C. Chem Rev 2016;116:5105–54.
[35] Neese F. Software update: the ORCA program system, version 4.0 WIREs. Comput Mol Sci 2017;e1327. https://doi.org/10.1002/wcms.1327.
[36] Pritchard Benjamin P, Altarawy Doaa, Didier Brett, Gibson Tara D, Windus Theresa L. New Basis Set Exchange: An Open, Up-to-Date Resource for the Molecular Sciences Community. J Chem Inf Model 2019;59(11):4814–20. https://doi.org/10.1021/acs.jcim.9b00725.
[37] Small D, Rosokha SV, Kochi JK, Head M. Characterizing the Dimerizations of Phenalenyl Radicals by ab Initio Calculations and Spectroscopy: σ-Bond Formation versus Resonance π-Stabilization. J Phys Chem A 2005;109:11261–7.
[38] Wang H. Formation of nascent soot and other condensed-phase materials in flames. Proc Combust Inst 2011;33:41–67.
[39] Bredas J-L. Mind the gap!. Mater Horiz 2014;1:17–9.
[40] Menon A, Dreyer JAH, Martin JW, Akroyd J, Robertson J, et al. Optical band gap of cross-linked, curved, and radical polyaromatic hydrocarbons. PCCP 2019;21(29):16240–51.
[41] Chen D, Wang H. HOMO–LUMO Gaps of Homogeneous Polycyclic Aromatic Hydrocarbon Clusters. J Phys Chem C 2019;123(45):27785–93.
[42] Commodo M, De Falco G, Bruno A, Borriello C, Minutolo P, D'Anna A. Physicochemical evolution of nascent soot particles in a laminar premixed flame: from nucleation to early growth. Combust Flame 2015;162:3854–63.
[43] Sirignano M, Collina A, Commodo M, Minutolo P, D'Anna A. Detection of aromatic hydrocarbons and incipient particles in an opposed-flow flame of ethylene by spectral and time-resolved laser induced emission spectroscopy. Combust Flame 2012;159:1663–9.
[44] Mercier X, Carrivain O, Irimiea C, Faccinetto A, Therssen E. Dimers of polycyclic aromatic hydrocarbons: the missing pieces in the soot formation process. PCCP 2019;21:8282–94.
[45] Adkins EM, Giaccai JA, Miller JH. Computed electronic structure of polynuclear aromatic hydrocarbon agglomerates. Proc Combust Inst 2017;36:957–64.